Renewable Energy 54 (2013) 235–240

Contents lists available at SciVerse ScienceDirect

Renewable Energy

journal homepage: www.elsevier.com/locate/renene

Velocity interference in the rear rotor of a counter-rotating wind turbine

Seungmin Lee [a,1], Eunkuk Son [a,2], Soogab Lee [a,b,*]

[a] Department of Mechanical and Aerospace Engineering, Seoul National University, South Korea
[b] Institute of Advanced Aerospace Technology, Seoul National University, South Korea

ARTICLE INFO

Article history:
Received 6 February 2012
Accepted 1 August 2012
Available online 13 August 2012

Keywords:
Counter-rotating wind turbine
Velocity interference
Induction factor
Power coefficient
Thrust coefficient
Vortex lattice method

ABSTRACT

A counter-rotating wind turbine having two rotors rotating in opposite directions on the same axis is proposed to improve the aerodynamic performance of a wind turbine. In order to predict the aerodynamic performance of the counter-rotating wind turbine, the inflow interference in its rear rotor by the wake of the front rotor needs to be considered because the rear rotor operates inside the wake of the front rotor. In the previous research, the rear rotor was assumed to operate inside the fully developed stream tube of the front rotor to define the inflow condition on the rear rotor. In this study, to consider simultaneously the aerodynamic interaction between the two rotors of the counter-rotating wind turbine without any assumption on the inflow velocity of the rear rotor, an aerodynamic analysis of the counter-rotating wind turbine was carried out by using a free-wake vortex lattice method. The power coefficient and the wake geometry of the counter-rotating wind turbine were compared with those of a single rotor wind turbine, and the induction factors on the rear rotor were compared with that from the BEMT, assuming that the rear rotor operated inside the fully developed stream tube of the front rotor.

1. Introduction

The horizontal axis wind turbine, which has a single rotor and three blades, has been widely used as the conventional type of wind turbines. However, various other types of wind turbines have been proposed for improvement of power efficiency and suitability for low wind speeds [1].

A counter-rotating wind turbine has been proposed as a new design for improvement of power efficiency. Its configuration consists of two rotors rotating in opposite directions on the same axis. According to the momentum theory by Newman [2], the ideal maximum power coefficient of a wind turbine having a single rotor is about 59%, but that of a wind turbine having two rotors is about 64%, which is about 5% improvement. Based on this result, several experimental studies on the counter-rotating wind turbine have been carried out to ultimately extract more power from the wind [3–7].

In order to minimize the rising costs arising from the additional rotor of the counter-rotating wind turbine and at the same time to maximize the energy efficiency, an aerodynamic design of a counter-rotating wind turbine having the same solidity as a wind turbine having a single rotor was required. For the aerodynamic design, an efficient and reliable method to predict the aerodynamic performance for the counter-rotating wind turbine was needed. Especially, the prediction method would need to consider the interaction between the two rotors of the counter-rotating wind turbine, which would not have been considered for a wind turbine having a single rotor. However, most of the previous studies for the counter-rotating wind turbine have been limited experiments, leaving only few numerical studies on the counter-rotating wind turbine.

The blade element momentum theory (BEMT), which has been widely used for the aerodynamic design of the conventional wind turbine, cannot be directly applied in the prediction of the counter-rotating wind turbine. Therefore, some assumptions for the interaction between the two rotors of the counter-rotating wind turbine are needed. In the previous research [8] by using the BEMT, it was assumed that the rear rotor operates inside the fully developed stream tube of the front rotor in the calculation of the induced velocity on the rear rotor of the counter-rotating wind turbine. This assumption, however, has some limitations: the inflow velocity on the rear rotor is excessively reduced and the wake from the rear rotor does not affect the inflow on the front rotor. Therefore, in order to predict a more accurate performance of the counter-rotating wind turbine, the interaction between the front and the rear rotor of the

* Corresponding author. Rm. 105, Bldg. 311, Seoul National University, Seoul 151-744, South Korea. Tel.: +82 2 880 7384; fax: +82 2 875 4360.
E-mail address: solee@snu.ac.kr (S. Lee).
[1] Rm. 105, Bldg. 311, Seoul National University, Seoul 151-744, South Korea. Tel.: +82 2 880 7384.
[2] Rm. 218, Bldg. 35, Seoul National University, Seoul 151-744, South Korea. Tel.: +82 2 880 7299.

0960-1481/$ – see front matter © 2012 Elsevier Ltd. All rights reserved.
http://dx.doi.org/10.1016/j.renene.2012.08.003

Nomenclature

a	Axial induction factor
$a_{i,j}$	Influence coefficient
BEMT	Blade element momentum theory
C_P	Power coefficient
C_T	Axial force coefficient
CRWT	Counter-rotating wind turbine
d	Distance between two rotors
L	Lift force
n	Normal vector
N_f	Number of vortex filaments
R	Rotor radius
r	Radial distance
U_∞	Wind velocity
v	Induced velocity
V_x	Axial velocity
x	Axial distance
Φ^*, Φ_∞	Total velocity potential and free stream potential, respectively
θ_{front}, θ_{rear}	Pitch angles of the front and rear rotor, respectively
Γ	Circulation
γ	Vorticity
λ	Tip speed ratio
ρ	Air density
Ψ	Blade azimuth angle
Subscript	
w	Wake

counter-rotating wind turbine should be considered simultaneously without any assumption about the inflow velocity on the rear rotor.

In this study, a free-wake vortex lattice method for the counter-rotating wind turbine is developed to consider simultaneously the interaction between the two rotors of the counter-rotating wind turbine without any assumption about the inflow velocity on the rear rotor. This method is validated by comparing its results with the experimental results [9] on the performance and the axial velocity of the wind turbine and is then applied to analyze the characteristics of the counter-rotating wind turbine. The power coefficient and the wake geometry of the counter-rotating wind turbine are compared with those of a wind turbine having a single rotor, and the induction factors on the rear rotor are compared with those from the BEMT based on the assumption that the rear rotor operates inside the fully developed stream tube of the front rotor.

2. Numerical method

For the aerodynamic analysis of the counter-rotating wind turbine, the free-wake vortex lattice method is used as shown in Fig. 1. In the case of a moderate tip Mach number, the continuity equation for the flow field around rotor blades is reduced to the Laplace's equation in terms of the total velocity potential:

$$\Phi^* = 1/4\pi \int_{\text{blade \& wake}} \gamma n \cdot \text{grad}(1/r)\text{dS} + \Phi_\infty \quad (1)$$

Applying the small disturbance assumption, rotor blades are replaced with flat plates, and then those are represented by vortex sheets that are the general solutions of the Laplace's equation [10]. The Neumann boundary condition, which is the non-penetration condition on the rigid blade surface, is applied to each sub-divided panel on the sheets, and then the vortex strength on each panel is calculated by solving the following linear algebraic equation:

$$a_{i,j}\Gamma_j + n_j(U_\infty + v_{w,j}) = 0 \quad (2)$$

where the sum of the normal velocity induced by the circulations of all the panels and the normal components of the wind velocity and the wake-induced velocity on each sub-divided panel becomes zero to satisfy the non-penetration condition on the rigid blade surface.

After the solutions on the vortex strength are obtained from the Equation (2), the force generated by each vortex sheet is computed by using the Kutta–Joukowski theorem [10].

$$L_j = \rho v_j \Gamma_j \quad (3)$$

For computational efficiency of the free-wake calculation, the constant vorticity contour model [11] was used to represent the wakes released from the blades. The wake filaments having the same strength are distributed by the circulation distribution of the trailing edge and release points, which are the points of the wake filaments distributed at the trailing edge to be released into the wake, are changed with the azimuthal change of the circulation distribution. The computation cost for the free wake calculation is reduced by using the constant vorticity contour model because it generally needs only half the filaments used in the general vortex lattice wake model, in which the span-wise and azimuthal variations of the circulation distribution are represented by the trailed components and the shed components, respectively. The strength of the wake filaments in the constant vorticity contour model is determined as follows:

$$\Gamma_w = 1.5 \max\left[\Gamma_w(r,\psi)/(N_f/2)\right] \quad (4)$$

where $\Gamma_w(r,\Psi)$ is the bound circulation distribution and N_f is the number of wake filaments to be trailed from blades. Furthermore, the factor of 1.5 is used to leave a margin to consider that the maximum circulation can grow in the free-wake calculation.

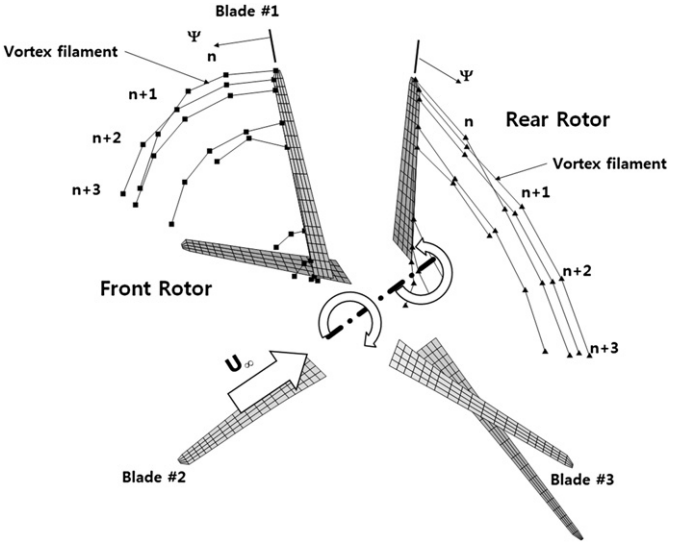

Fig. 1. Free-wake vortex lattice model for a counter-rotating wind turbine.

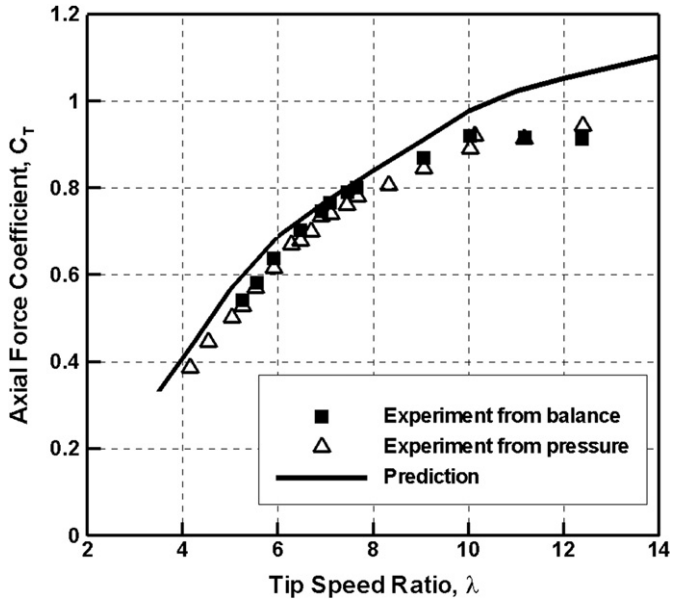

Fig. 2. Axial force coefficient as a function of tip speed ratio.

In order to compute the release point, radial locations where the bound circulation reaches the levels that bound the half-integral multiples of the strength of the wake filaments are determined and then linear interpolation is used to define the release point inside the interval as follows:

$$r_n = r_a + [(n+0.5)\Gamma - \Gamma_w(r_a)](r_b - r_a)/(\Gamma_w(r_b) - \Gamma_w(r_a)) \quad (5)$$

Moreover, in order to predict efficiently the induced velocities by wakes from the wind turbine, curved vortex elements were used. Because the wakes generated from the wind turbine have helical shapes, the induced velocity calculated by using the curved vortex elements is more accurate and efficient than that calculated by using straight-line elements for the same number of points representing the wake geometry. For the curved vortex elements, the approximate Biot–Savart integration for a parabolic arc filament shape is applied to the free-wake calculation [12].

The time-marching free-wake method was applied to the wake convection, and the wake position was updated by using the induced velocity calculated by the second-order backward difference at every time step.

$$x_{n+1} = x_n + 0.5\Delta t(3v_n - v_{n-1}) \quad (6)$$

By using the free-wake vortex lattice method for the counter-rotating wind turbine, the induced velocity in the flow field of the counter-rotating wind turbine is directly calculated and the interaction between the two rotors was considered simultaneously without any assumption about the inflow velocity on the rear rotor.

3. Results and discussion

For a validation of the free-wake vortex lattice method used here, predicted results were compared with the experimental results [9,13] in EU project MEXICO (Model Rotor Experiments in Controlled Conditions). An experiment was carried out under controlled conditions to provide an extensive experimental database for a wind turbine in the Large Low-speed Facility (LLF) of German Dutch Wind Tunnel DNW in 2006. The experimental wind turbine for the wind tunnel test was a three-bladed wind turbine of 4.5 m diameter. Its design tip speed ratio was 6.5 and a tapered and twisted blade was used. DU 91-W2-250, RISØ A1-21 and NACA 64–418 were used for the airfoils at the root, mid-span and outer part of the blade, respectively. The operation condition for the comparison was the axisymmetric condition in which the rotor speed was 424.5 rpm, tip speed was 100 m/s, and the pitch angle was −2.3°.

In Fig. 2, the axial force coefficients as a function of the tip speed ratio are compared with the measurements. In the experiment, the axial force coefficients were measured in two ways, by using the balance at the tower with a correction for the tower drag and by integration of the pressure distribution along the blade. While the axial force coefficient is slightly over-predicted at some high tip speed ratios, predictions agree well with the measurements overall.

The power coefficients as a function of the tip speed ratio are compared with the measurements in Fig. 3. Although the power coefficient is slightly over-predicted, the maximum power coefficient is obtained at the design tip speed ratio, and the overall shape of the curve of the power coefficients follows that of the curve of the measurements.

For the analysis of the counter-rotating wind turbine, the axial velocity decay behind the rotor plane should be predicted accurately because the rear rotor operates inside the wake from the front rotor of the counter-rotating wind turbine. In Fig. 4, the axial velocity decay at $r/R = 0.82$ is compared with the measurements. The rotor is located at the axial position zero and positive axial position means a position downstream from the rotor plane in the figure. The axial velocities at the rotor plane and at a position downstream agree well with the measurements.

After the numerical method was validated with respect to its predictions on aerodynamic performance and downstream velocity field, it was extended to the analysis of the counter-rotating wind turbine. The MEXICO rotor that was used for the validation was applied to both front and rear rotors, and the same rotating speed was applied to both rotors.

In Figs. 5 and 6, the axial velocity contour and the vorticity contour of the counter-rotating rotors were compared with those of the single rotor. The rear rotor was located at half the radius of the counter-rotating rotor behind the front rotor and the tip speed ratio was 6.5. The axial velocity of the flow that passed the front rotor was reduced again by the rear rotor. The axial velocity in the far

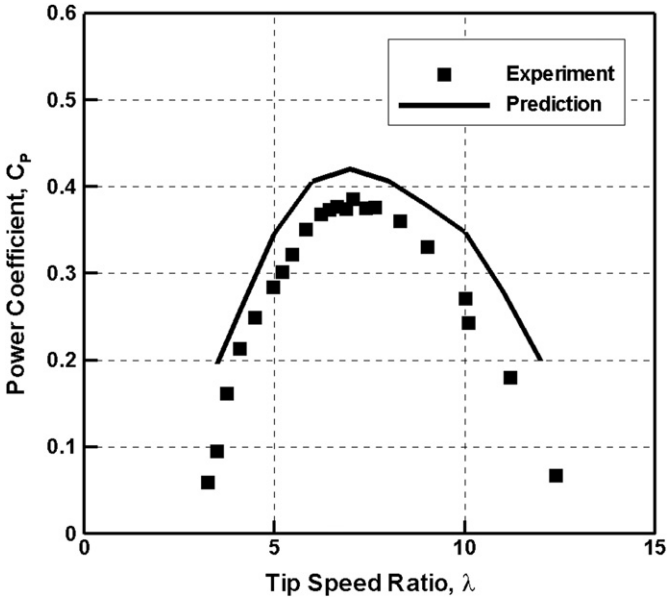

Fig. 3. Power coefficient as a function of tip speed ratio.

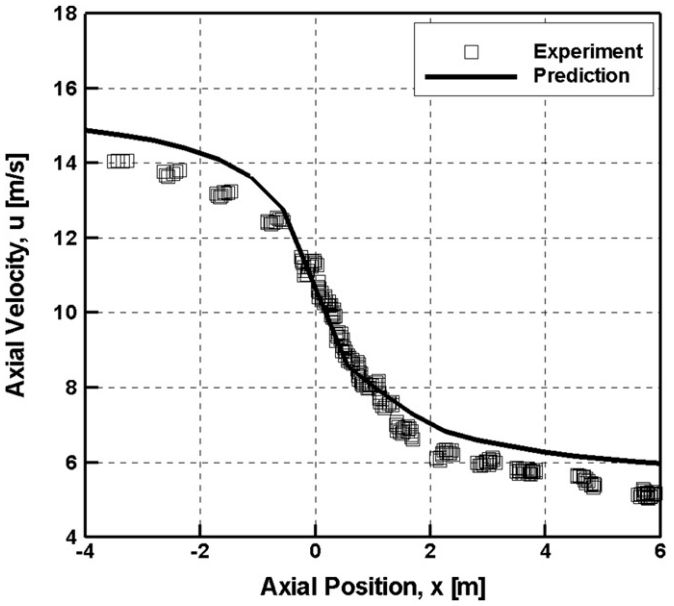

Fig. 4. Axial velocity decay at $r/R = 0.82$.

downstream of the counter-rotating rotor was much lower than that of the single rotor. The tip vortices generated by each of the counter-rotating rotors are shown in Fig. 6. Due to the axial velocity reduction by the rear rotor, tip vortex trajectory of the front rotor is more radially expanded than that of the single rotor.

In order to compare the tip vortex trajectories of each rotor, the tip vortex locations were obtained from the vorticity contours, as shown in Fig. 7. In this figure, the tip vortex trajectories for the axial distance from each rotor plane are compared. The tip vortex trajectories of both the front and rear rotor are more expanded radially than those of the single rotor due to the axial velocity reduction of the counter-rotating rotor. As the tip vortex goes downstream, the convection velocity of the tip vortex from the front rotor becomes higher than that of the single rotor due to the additional velocity induced by the tip vortices of the rear rotor. On the contrary, because the velocity induced by the tip vortices of the front rotor acts in the opposite direction to the tip vortex from the rear rotor, the convection velocity of the tip vortex from the rear rotor is much lower than that of the single rotor.

In Fig. 8, the power coefficient according to the pitch combination of the counter-rotating rotor is compared. The maximum power coefficient is obtained at a lower tip speed ratio than that of the single rotor because the rotor's solidity increased in the case of the counter-rotating rotor. The maximum power coefficients vary

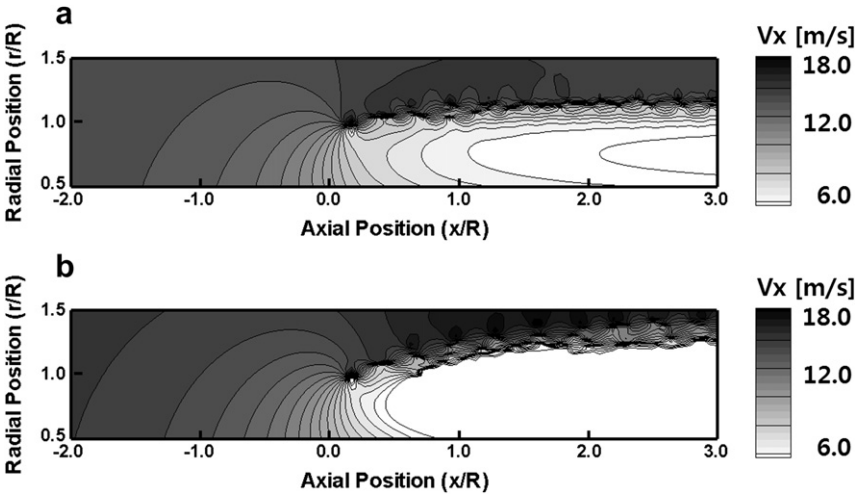

Fig. 5. Axial velocity contour ($\lambda = 6.5$): (a) single rotor, (b) counter-rotating rotor ($d/R = 0.50$).

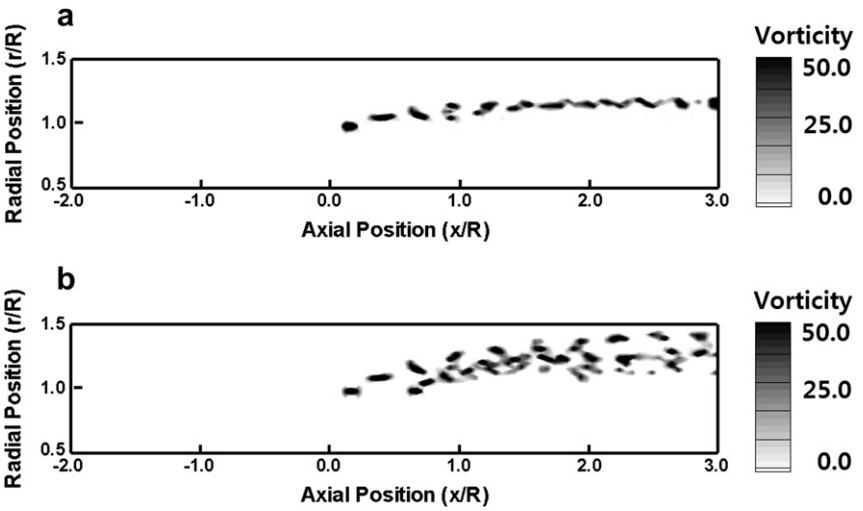

Fig. 6. Vorticity contour ($\lambda = 6.5$): (a) single rotor, (b) counter-rotating rotor ($d/R = 0.50$).

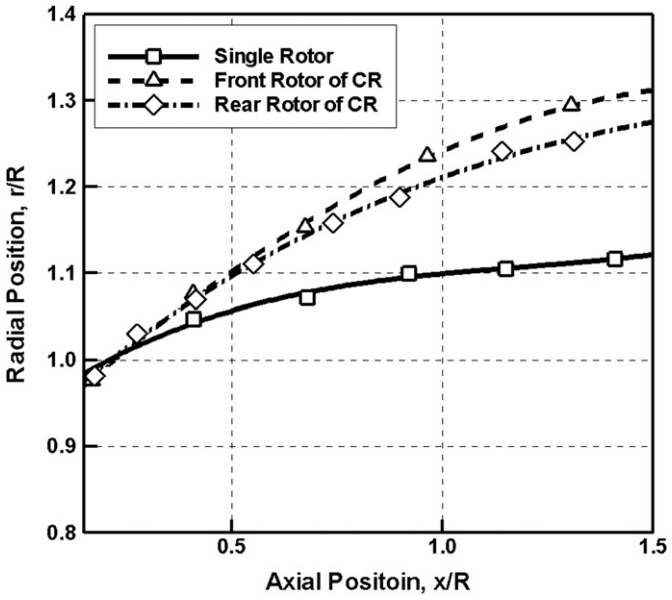

Fig. 7. Tip vortex trajectory ($\lambda = 6.5$, $d/R = 0.50$).

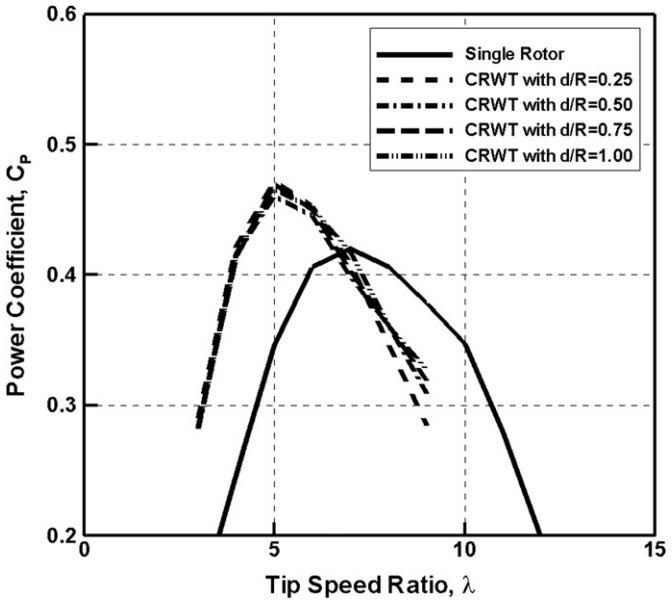

Fig. 9. Power coefficient variation according to the distance between the two rotors of the counter-rotating wind turbine ($\theta_{front} = \theta_{rear} = 0.0^\circ$).

according to the pitch combination of the counter-rotating rotor, and the maximum is obtained when both pitch angles are zero in the case of the rotor used in this study. In this case, the maximum power coefficient of the counter-rotating rotor is about 0.47, which is an increase of 12% from that of the single rotor whose maximum power coefficient is 0.42.

The power coefficient variation according to the distance between the two rotors of the counter-rotating wind turbine is shown in Fig. 9. Both the pitch angles of the two rotors were set to zero at which the maximum power coefficient was obtained, and the non-dimensional distances between the two rotors, d/R, were 0.25, 0.5, 0.75 and 1.0. Although the distance between the two rotors varies considerably, the power coefficient is little changed.

In order to investigate how much effect distance change has on the power coefficient, the power coefficient of each rotor according to the distance between the two rotors is shown in Fig. 10. As the distance increases, the power coefficient of the front rotor increases but that of the rear rotor decreases. In this case, the velocity interference on the rear rotor is reduced and the velocity on the front rotor is recovered, so the power coefficient of the front rotor increases. However, as the distance increases, velocity decay behind the front rotor increases and the velocity on the rear rotor is reduced, so the power coefficient of the rear rotor decreases. Because the increase and decrease of the power coefficient of the two rotors cancel each other out, the total power coefficient, which is the sum of the power coefficients of the two rotors, is little changed.

In Fig. 11, the axial induction factors at $r/R = 0.82$ according to the distance between the two rotors of the counter-rotating wind turbine are compared. Regardless of the distance between the two

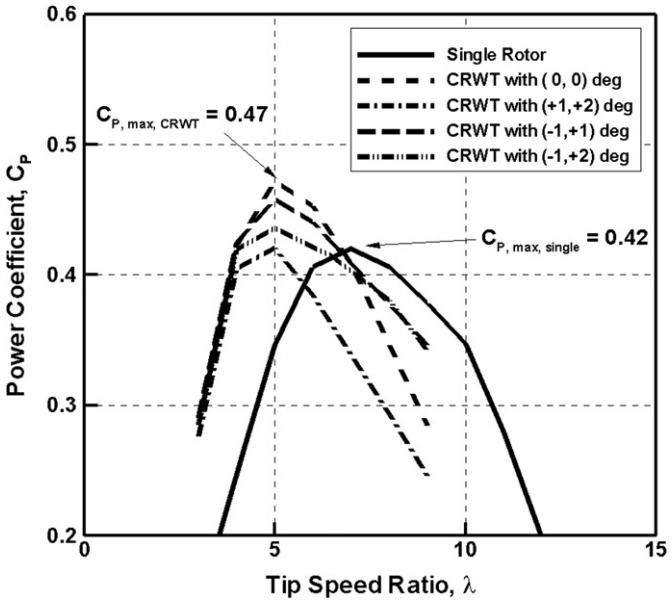

Fig. 8. Power coefficient variation according to the pitch combination of the counter-rotating wind turbine ($d/R = 0.25$).

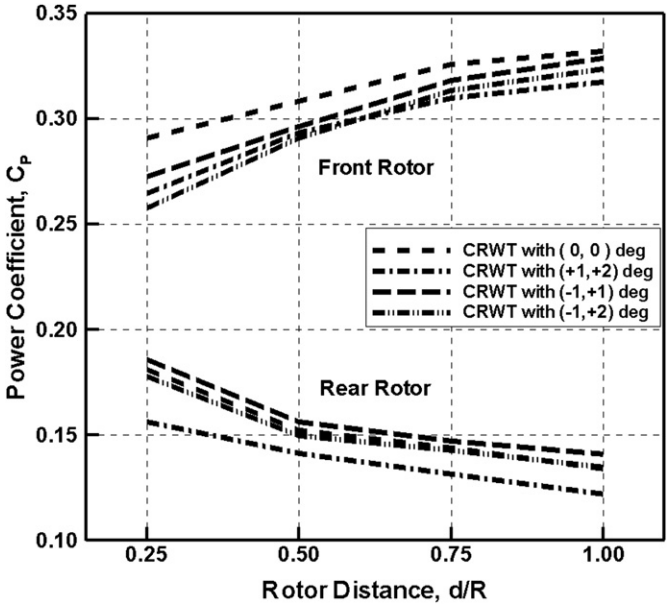

Fig. 10. Power coefficient variation of the front and rear rotor according to the distance between the two rotors of the counter-rotating wind turbine.

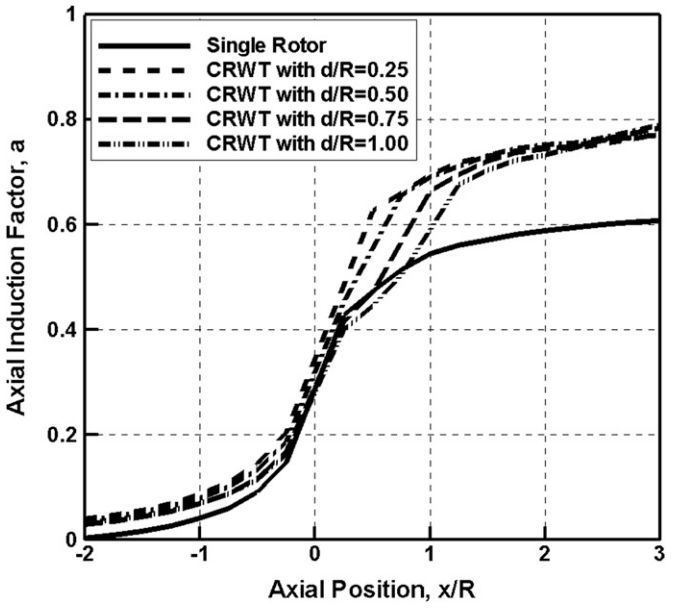

Fig. 11. Axial induction factor at $r/R = 0.82$ according to the distance between the two rotors of the counter-rotating wind turbine ($\theta_{front} = \theta_{rear} = 0.0^{\circ}$).

Table 1
Axial induction factor on each rotor plane and its ratio.

	Free-wake vortex lattice method			BEMT	
	Axial induction factor		Ratio	Ratio ($a_{rear} = 0.20$)	Ratio ($a_{rear} = 0.33$)
	Front rotor	Rear rotor			
$d/R = 0.25$	0.35	0.49	1.41	2.18	2.30
$d/R = 0.50$	0.32	0.55	1.73	2.23	2.38
$d/R = 0.75$	0.29	0.57	1.95	2.29	2.48
$d/R = 1.00$	0.28	0.59	2.10	2.31	2.52

rotors, all of the counter-rotating rotors have similar axial force coefficients of about 0.95 in these cases. For this reason, the axial induction factors at far downstream become similar, although the axial induction factors around the rotor planes are different. Moreover, the axial induction factor on the front rotor decreases but that on the rear rotor increases as the distance between the rotors increases.

The axial induction factors on each rotor plane are shown in Table 1. In order to estimate the effect of the distance between the rotors on the axial induction factor of the rear rotor, the ratio of the axial induction factor of the rear rotor to that of the front rotor was used. As the distance increases, the ratio increases because the interference of the rear rotor on the front rotor decreases but the velocity decay on the rear rotor increases. The ratios obtained by the BEMT, based on the assumption that the rear rotor operates inside the fully developed stream tube of the front rotor, are also compared with the ratio from the free-wake vortex lattice method. As the distance decreases, the discrepancy between the ratios of the BEMT and the free-wake vortex lattice method grows, so the fully developed stream tube assumption BEMT can be applied in limited cases.

4. Conclusion

In this study, a free-wake vortex lattice method for the counter-rotating wind turbine was developed to consider simultaneously the interaction between the two rotors without any assumption about the inflow velocity on the rear rotor.

This method was validated by comparing its results with the experimental results in EU project MEXICO with respect to the performance and the axial velocity of the wind turbine, and was applied to analyze the characteristics of the counter-rotating wind turbine.

The wake geometry and the power coefficient of the counter-rotating wind turbine were compared with those of wind turbine having a single rotor. The tip vortex trajectories of both the front and rear rotors were more expanded radially than those of the single rotor. Moreover, the convection velocity of the tip vortex from the front rotor became higher than that of the single rotor but that of the tip vortex from the rear rotor was much lower than that of the single rotor. The maximum power coefficient of the counter-rotating rotor was increased by 12% from that of the single rotor. Because the increase and decrease of the power coefficient of the two rotors canceled each other out, the total power coefficient was little changed with distance between the two rotors. The induction factors on the rear rotor were compared with those from the BEMT, which was based on the assumption that the rear rotor operates inside the fully developed stream tube of the front rotor, and it was found that this assumption can be applied in very limited cases when the distance between the two rotors of the counter-rotating wind turbine decreases.

Acknowledgment

This work was supported by the Human Resources Development and the New and Renewable Energy of the Korea Institute of Energy Technology Evaluation and Planning (KETEP) grant funded by the Korea government Ministry of Knowledge Economy (No. 20094020100060 & 20104010100490).

References

[1] Hau E. Wind turbines – fundamentals, technologies, application, economics. 2nd ed. , Berlin: Springer; 2006.
[2] Newman BG. Actuator-disc theory for vertical-axis wind turbines. Journal of Wind Engineering and Industrial Aerodynamics 1983;15:347–55.
[3] Appa K. Energy innovations small grant (EISG) program (counter rotating wind turbine system) [Final report]. California, US: EISG; 2002.
[4] Jung S, No T, Ryu K. Aerodynamic performance prediction of a 30kW counter-rotating wind turbine system. Renewable Energy 2005;30:631–44.
[5] Kanemoto T, Galal AM. Development of intelligent wind turbine generator with tandem wind rotors and double rotational armatures [Series B]. JSME International Journal 2006;49(No. 2):450–7.
[6] Shen WZ, Zakkam VAK, Sorensen JN, Appa K. Analysis of counter-rotating wind turbines. Journal of Physics 2007 [Conference series 75].
[7] Jang TJ, Heo HK. Study on the development of wind power system using mutually opposite rotation of dual rotors. Proceedings of the Renewable Energy 2008.
[8] Lee S, Kim H, Son E, Lee S. Effects of design parameters on aerodynamic performance of a counter-rotating wind turbine. Int'l symposium on low carbon & renewable energy technology (ISLCT 2010); 2010.
[9] Schepers JG, Boorsma K, Bon A, Kim C, Cho T. Results from Mexnext: analysis of detailed aerodynamic measurements on a 4.5m diameter rotor placed in the large German Dutch wind tunnel DNW. Brussels, Belgium: EWEA; 14–17 March 2011.
[10] Katz J, Plotkin A. Low-speed aerodynamics. 2nd ed. Cambridge University Press; 2001.
[11] Quackenbush TR, Wachspress DA, Alexander H. Rotor aerodynamic loads computation using a constant vorticity contour free wake model. Journal of Aircraft 1995;32(No. 5):911–20.
[12] Bliss DB, Teske ME, Quackenbush TR. A new methodology for free wake analysis using curved vortex elements [Contractor report 3958]. NASA; 1987.
[13] Schepers JG, Snel H. Model experiments in controlled conditions [Final report ECN-E-07-042]. ECN; 2007.